Summer Project Report
May-July 2014
Laboratory for Quantum Magnetism
Ecole polytechnique federale de Lausanne, Switzerland

AC Magnetoelectrical Susceptibility Study of Multiferroics

Abhisek Datta

5^{th} *Year, 5-Year Integrated MSc*
Department of Physics
Indian Institute of Technology Kharagpur, Kharagpur-721 302, West Bengal, India

---

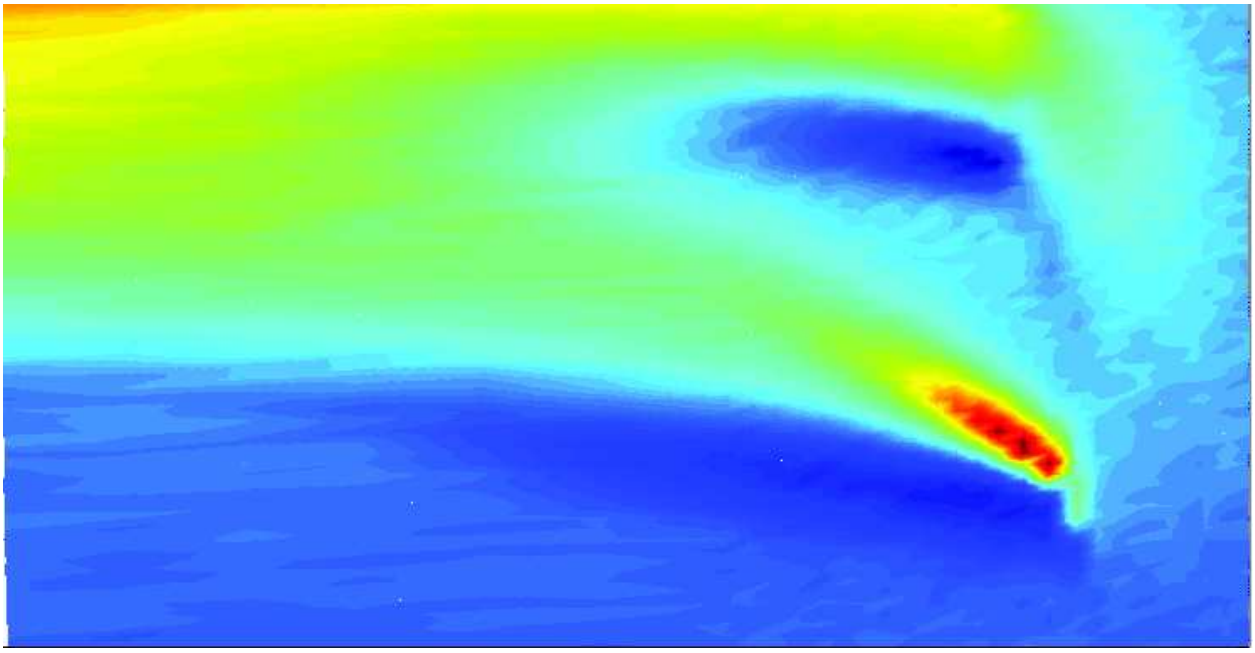

4 September 2014

Contents

Abstract

Multiferroics are materials in which ferroelectric and magnetic e.g., ferromagnetic or antiferromagnetic orders co-exist. Some of these show the magnetoelectric effect which is the coupling between electric and magnetic degrees of freedom leading to induction of electric polarization by an applied magnetic field and also induction of magnetic polarization by an applied electric field. Multiferroic substances have attracted attention in recent times as they are expected to show relatively larger magnetoelectric effect than others. $TbMnO_3$ and $DyMnO_3$ are prototypical magnetoelectric multiferroics where ferroelectricity develops due to a magnetic phase transition to a spiral magnetic ordered phase. Cu_2OSeO_3 is another magnetoelectric material and is the only one in which magnetoelectric (ME) susceptibility dM/dE (i.e. the change in magnetization by the application of an AC electric field) measurements have been performed to successfully map the magnetoelectric phase diagram. During this work, dM/dE measurements were used to map the phase diagram of Cu_2OSeO_3 for directions of applied magnetic and electric fields different from that reported so far. This success in Cu_2OSeO_3 thus became the motivation to make similar attempts on $TbMnO_3$ and $DyMnO_3$. The samples were first oriented to identify the crystallographic axes, then DC magnetic susceptibility and AC magnetoelectric susceptibility measurements were carried out. The DC magnetization measurements for $TbMnO_3$ showed clear signatures of phase transitions and thus subsequently dM/dE measurements were performed with an AC applied electric field in order to perform a sensitive probe of the phase diagram. But for $TbMnO_3$, dM/dE response could not be observed in any portion of the phase diagram i.e. at different magnetic field and temperature. This entire procedure from Cu_2OSeO_3 to the manganates have been presented here in this report.

1 Introduction

1.1 Magnetoelectric effect

Magnetoelectric effect refers to the coupling between magnetic and (ferro)electric orders due to which there is induction of electric polarization due to an applied magnetic field and a magnetization due to an applied electric field. Using this magnetoelectric effect, there can be new device applications such as memory devices. The magnetoelectric effect can be written in forms of $P_i(H_j)$ or $M_i(E_j)$ as :

$$P_i = \alpha_{ij} H_j + \frac{\beta_{ijk}}{2} H_j H_k + ... \tag{1}$$

$$\mu_0 M_i = \alpha_{ji} E_j + \frac{\gamma_{ijk}}{2} E_j E_k + ... \quad (2)$$

where P_i and M_i are the components of electric polarization and magnetization, α, β and γ are tensors representing the magnetoelectric coefficients. A detailed description is given by Eerenstein et al. (2006).

Multiferroics are materials in which ferroelectric and ferromagnetic (or antiferromagnetic) orders coexist in the same phase. As ferromagnetic (ferroelectric) materials show large response to magnetic (electric) fields, multiferroics can be expected to show a large magnetoelectric response as well.

The magnetoelectric effect has been studied for more than four decades now, but the weak coupling between ferroelectricity and magnetism has made it difficult to use it for practical applications. The magnetoelectric interactions were too weak in the substances studied earlier, mainly because the temperature scale for ferroelectric order is much higher than that for magnetic order. But later on some rare earth manganites like $TbMnO_3$ and $DyMnO_3$ were found to give a large magnetoelectric response (change in electric polarization by applying magnetic field). This revived the interest again in the study of magnetoelectric multiferroics.

There can be various mechanisms to explain the magnetoelectric effect in different materials. For example, the magnetoelectric coupling in rare earth manganites like $TbMnO_3$ is due to a noncollinear (namely cycloidal) spiral spin structure (Kimura , 2007). Also the magnetoelectric effect in materials like Cu_2OSeO_3 is due to different mechanism and is explained by Seki et al. (2012). The following sub-section details on the magnetoelectric effect in rare earth manganites as they are main focus of this project for the magnetoelectric susceptibility study.

1.2 Rare Earth Manganites

Large magnetoelectric response has been observed in rare earth manganites like $TbMnO_3$ and $DyMnO_3$. Kimura et al. (2003) reports the discovery of ferroelectricity in $TbMnO_3$ and Goto et al. (2004) for the same in $DyMnO_3$ These rare earth manganites have antiferromagnetic (AFM) orders with long wavelength and ferroelectricity is said to be originated due to competing magnetic interactions. A more detailed description of the magnetic structures and magnetoelectric study of these rare earth manganites has been given by Kimura et al. (2005) and Kimura (2007).

For $TbMnO_3$, it has an orthorhombically distorted perovskite structure. The Mn moments in $TbMnO_3$ undergo an AFM transition at $T_N(Mn) \sim 41\ K$. The Mn moments are aligned along the b-axis and show a sinusoidal order with a propagation vector along the b-axis.

The propagation vector decreases with decreasing temperature and becomes locked in at $T_{lock} \sim 28\ K$. It is at this temperature that the collinear sinusoidal magnetic ordering of the Mn ions change to a non-collinear spiral magnetic ordering, cycloidal in this case. And also it is at this temperature that ferroelectricity appears in this material. In $TbMnO_3$ ferroelectric order develops with spontaneous polarization along the c-axis. On lowering the temperature, the Tb moments then undergo AFM transition at $T_N(Tb) \sim 7\ K$.

Similarly in $DyMnO_3$, the transition temperature for the Mn ions is $T_N(Mn) \sim 39\ K$, and they also have sinusoidal AFM ordering of the Mn moments. Ferroelectricity develops in this material below $\sim 18\ K$ which is also the temperature at which the propagation vector locks in T_{lock}. The spontaneous polarization in this case is along the b-axis. Also the AFM transition temperature of Tb ions $T_N(Tb)$ is below 10 K.

Thus it can be seen that ferroelectricity in these rare earth manganites is induced due to some sort of magnetic ordering, non-collinear spiral magnetic ordering in this case, which occurs below T_{lock} in these materials. Also as it has been shown by Kimura et al. (2005), this spontaneous electric polarization can be controlled and changed by applying a magnetic field. The key to understanding the magnetoelectric coupling in these materials is understanding the origin of this ferroelectric state. It is already known that ferroelectricity in $TbMnO_3$ is accompanied by the appearance of a spiral i.e. non-collinear magnetic structure. There are different types of spiral magnetic structures as shown in Kimura (2007), among which the cycloidal structure is most important for us, as this is the structure that develops in $TbMnO_3$ below T_{lock}. Cycloidal spiral structure is the arrangement where the spin rotation axis is perpendicular to the propagation vector of spiral. From recent theoretical studies, the general relation between the induced electric polarization and the magnetic moment for a spiral magnetic structure is given by :

$$\vec{P} \propto \gamma \vec{e_{ij}} \times (\vec{S_i} \times \vec{S_j}) \tag{3}$$

where γ is a constant proportional to the spin-orbit coupling and superexchange interactions, e_{ij} is along the propagation vector of the spiral structure and ($S_i \times S_j$) is parallel to the spin rotation axis. Therefore in $TbMnO_3$, since the spin rotation axis is along a and the propagation vector along b, the spontaneous polarization developed is along the c-axis. For $TbMnO_3$ in the phase with cycloidal spin structure, by the microscopic mechanism, the two adjacent non-collinearly coupled Mn moments displace the oxygen ions between them. This breaks the inversion symmetry and by the the inverse effect of the DM interaction (Dzyaloshinskii (1958) and Moriya (1960)), a local electric polarization is induced which is uniform and thus the total electric polarization is finite. A detailed description about this can be found in Kimura (2007).

1.3 Copper Selenide

Copper Selenide (Cu_2OSeO_3) is an insulating material which crystallizes in the chiral cubic space group $P2_13$. The magnetic ground state of Cu_2OSeO_3 is a proper screw with spins rotating within a plane perpendicular to the magnetic modulation vector q. The magnetic phase diagram of Cu_2OSeO_3 consists of helical, conical and skyrmion lattice phases. Seki et al. (2012) gives a detailed description of the magnetoelectric (ME) nature of skyrmions in Cu_2OSeO_3. Cu_2OSeO_3 has magnetically induced electric polarization in the ferrimagnetic, helimagnetic and the skyrmion lattice phase. The microscopic origin of the magnetoelectric coupling is identified to be due to $d-p$ hybridization mechanism as described in Seki et al. (2012). At low field and temperature, the magnetic phase diagram shows phase transitions between the helical and conical phase and also between the conical and the skyrmion phase. The skyrmion phase exists in the approximate temperature range of 56-58 K. In order to perform a more sensitive probe of the different phases and the phase boundaries between them, magnetoelectric susceptibility studies were carried out by applying an AC electric field which is described in Omrani et al. (2014). This kind of study is also presented here in a later section.

1.4 Magnetoelectric Susceptibility (dM/dE)

Thus till now, magnetic control over the ferroelectric properties of $TbMnO_3$ has been well studied and understood. The study of the electric control over its magnetic properties is also another interesting aspect that can be explored. Using SQUID magnetometry techniques, the variation of the magnetization of a sample with an applied AC electric field (magnetoelectric susceptibility) can be measured using a lock-in amplifier. If the applied AC electric field is $E = E_0 sin(\omega t)$ then the SQUID output voltage $V(E)$ can be written as :

$$V(E) = V(0) + \frac{dV(0)}{dE}E + \frac{1}{2}\frac{d^2V(0)}{dE^2}E^2 + O(E^3) \tag{4}$$

Now, since magnetization $M(E)$ is directly proportional to the SQUID signal $V(E)$, therefore the above equation can be written as :

$$M(E) = M(0) + \frac{dM(0)}{dE}E_0 sin(\omega t) + O(sin(2\omega t), sin(3\omega t), ...) \tag{5}$$

The input electric field is used as the reference for the lock-in amplifier, and thus the lock-in amplifier locks in at the ω frequency component and removes the DC part as well as

2ω, 3ω and other higher order terms. Therefore the output of the lock-in amplifier $L(E)$ is given by :

$$L(E) = A\frac{dM(0)}{dE}E_0 \tag{6}$$

where A is a proportionality constant. Then the magnetoelectric susceptibility is given by :

$$\frac{dM}{dE} = KL(E) \tag{7}$$

where K is another proportionality constant. Therefore, the magnetoelectric susceptibility $(\frac{dM}{dE})$ is directly obtained from the SQUID output voltage.

dM/dE measurements for Cu_2OSeO_3 (Omrani et al. , 2014) have been successful to conduct a study of the magnetic phase diagram, since it has shown distinctive responses in the different phases i.e. helical, conical, ferrimagnetic and the skyrmion phase, and at the different phase boundaries. The salient features include linear behaviour of dM/dE with different slopes in the conical phase, drop of the signal in the ferrimagnetic phase and the sharp peaks and dips at the boundaries of the skyrmion phase. Since both Cu_2OSeO_3 and the rare earth manganites are similar in the way that both host a magnetically induced electric polarization in phases with non-collinear spin structures, the rare earth manganites can also be expected to show dM/dE signals similar to Cu_2OSeO_3. $TbMnO_3$ has been widely studied and is known to have a strong dependence of the electric polarization on the magnetic field along all three crystal axis directions. Also the only spiral spin structure which showed very small dM/dE signals in Cu_2OSeO_3 was the helical phase, but in $TbMnO_3$ the spin structure in cycloidal where the spin rotation axis is perpendicular to the propagation vector of spiral which is suited for magnetoelectric coupling as given by Eqn 3.

Therefore, it may prove useful to conduct magnetoelectric susceptibility studies of rare earth manganites like $TbMnO_3$ and $DyMnO_3$. This will demonstrate whether the electric field affects the magnetic properties of these materials and if yes then it can be used to clearly identify the different magnetic phases for $TbMnO_3$ using the dM/dE responses like in Cu_2OSeO_3.

The next section gives the details about the magnetoelectric susceptibility study of Cu_2OSeO_3 conducted as a part of this project work. The latter sections presents the experiments performed on $TbMnO_3$ and $DyMnO_3$ starting from X-Ray Laue Method for determining the crystal axes to SQUID magnetometry to perform magnetization vs temperature measurements as well as to search for the dM/dE signals.

The two main experimental techniques used during this work were SQUID DC measurements and AC magnetoelectric susceptibility measurements.

1.5.1 DC Magnetic Susceptibility Measurements

A MPMS (Magnetic Property Measurement System) SQUID was used to conduct the DC magnetization measurements. The instrument is capable of conducting measurements by applying DC magnetic field (using superconducting magnets) till 5 T and to temperatures as low as 2 K. The samples are fixed in a tube and attached to a sample tube and inserted inside the sample chamber. The magnetization induced in the sample is measured by the SQUID and measurements can be taken by varying either the temperature or the magnetic field. For $TbMnO_3$ and $DyMnO_3$, DC magnetization was measured with this MPMS system by varying the temperature to obtain the M-T curves. Measurements were performed both for zero field cooled (ZFC) and field cooled (FC) states. A degaussing process (applying an damped oscillating magnetic field to remove any remnant magnetization in the sample) was generally carried out before doing the ZFC measurements.

1.5.2 AC Magnetoelectric Susceptibility Measurements

AC magnetoelectric (ME) susceptibility measurements were carried out using a S700X SQUID system from Cryogenic Ltd. This instrument is capable of conducting measurements by applying DC magnetic field till 7 T and to temperatures as low as 1.5 K. To measure the AC ME susceptibility, an AC electric field is applied on the faces of a single crystal sample using copper electrodes, and in the presence of a simultaneous DC magnetic field, the associated change in the sample magnetization is monitored directly using a SQUID magnetometer. Since the electric and magnetic fields need to be applied in specific directions, the crystal axis directions should be known before performing the measurements. The SQUID signal is recorded using a lock-in amplifier. As shown in the previous section by Eqn 7, the ME susceptibility dM/dE is directly proportional to the lock-in output signal. Thus the dM/dE measurements were performed for Cu_2OSeO_3 under different conditions of temperature and pressure to obtain the magnetic phase diagram. Also the same techniques were used with $TbMnO_3$ in an attempt to observe similar response of ME susceptibility as Cu_2OSeO_3.

2 Magnetoelectric Susceptibility study of Copper Selenide

AC magnetoelectric susceptibility studies on Cu_2OSeO_3 have been previously done by Omrani et al. (2014). Similar study was done here for a Cu_2OSeO_3 sample to confirm the experimental procedure used in this work. Also the magnetic phase diagram was mapped for electric and magnetic field directions different from that reported by Omrani et al. (2014).

2.1 Sample Characterization

Cu_2OSeO_3 crystallizes in the cubic space group and the sample piece of Cu_2OSeO_3 here was a rectangular shaped one with one known crystal axis direction - [111]. In order to determine the other two axis directions, X-Ray Laue method (described in Appendix 6.1) was performed on the sample. By matching the Laue patterns obtained from the three perpendicular surfaces of the sample with the known Laue patterns, the other two crystal axis directions were identified to be $[1\bar{1}0]$ and $[\bar{1}\bar{1}2]$. The Laue patterns obtained by the Laue method for the Cu_2OSeO_3 sample are given in Figure 1.

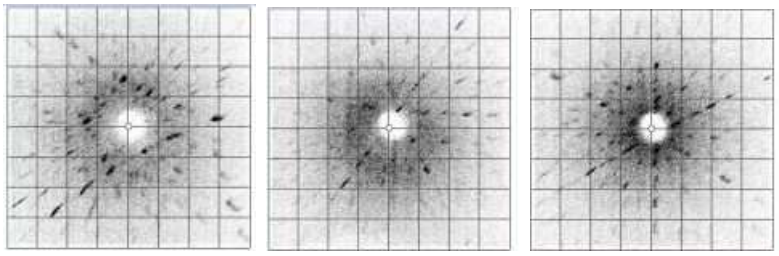

Fig. 1. *Laue patterns for* Cu_2OSeO_3. *The first figure is for* $[\bar{1}\bar{1}2]$ *direction, the second figure is for* $[1\bar{1}0]$ *directions and the third figure is for* [111] *direction. The X-Rays were produced using V=10 kV and I=20 mA in the power supply*

So all the three axis directions are now known for the sample which is required for performing the dM/dE measurements. The crystal axis orientations and the current shape of the sample are shown in Figure 2.

The mass of this Cu_2OSeO_3 sample was measured to be 5.1 mg. The orientation for the dM/dE measurement was chosen to be - $E \parallel [111]$ and $B \parallel [1\bar{1}0]$ i.e. the electric and magnetic field were applied perpendicular to each other. In order to achieve this the copper electrodes were to be connected on the surfaces which were normal to the [111] axis.

The process of preparing the sample for the measurement involved first attaching thin copper foils as electrodes on the [111] surfaces with the use of low temperature varnish and then baking it in the oven till 120^o C followed by cooling it for around thirty minutes. This hardens the varnish and fixes the copper electrodes on the surfaces of the sample.

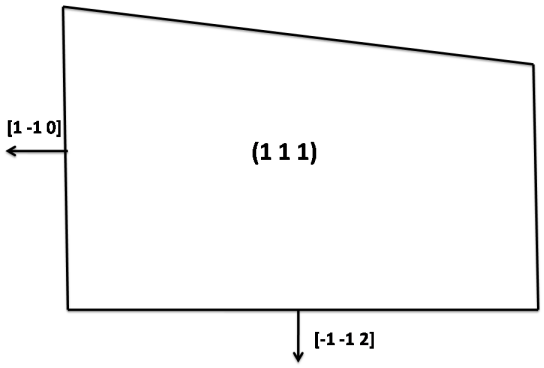

Fig. 2. *Shape of the* Cu_2OSeO_3 *sample piece with the axis directions. The* [111] *direction shown in the figure is out of the plane*

Next, the electrodes are soldered to the wires of the sample rod through which the electric field will be applied. The sample is attached in a way such that the $[1\bar{1}0]$ surface is along the sample rod so that the magnetic field applied will be along the $[1\bar{1}0]$ direction. The distance between the copper electrodes for the prepared sample was measured to be 0.94 mm. The sample is thus prepared for the measurement and is put inside the instrument for ME susceptibility measurement.

2.2 dM/dE measurements and Phase Diagram

ME susceptibility measurements were performed on the Cu_2OSeO_3 sample described above by applying the AC electric field along the [1 1 1] direction and the DC magnetic field along the [1 $\bar{1}$ 0] direction. The ME susceptibility was measured with the help of the lock-in amplifier (as described in section 1.4) for different conditions of magnetic field and temperature. The lock-in amplifier gives both the real and imaginary parts of the ME susceptibility and their variation with magnetic field at different temperatures are given in figures 3, 4 and 5. The y-axis in the figures give dM/dE where E is the AC electric field applied.

Figure 3 shows the variation of dM/dE with magnetic field at temperatures below 56 K. It is known that there is no skyrmion phase below 56 K, and also that ME coupling is weak in helical phase and much stronger in conical as discussed in previous sections. From the figure it is seen that the dM/dE signal is nearly zero in the beginning i.e. till B 0.01 T(which marks the helical phase), and then increases with magnetic field (marking the conical phase). Thus the transition from helical to conical phase occurring at around 0.01 T for temperatures below 56 K can be understood from this figure.

Figure 4 shows the variation of dM/dE with magnetic field at temperatures between 56

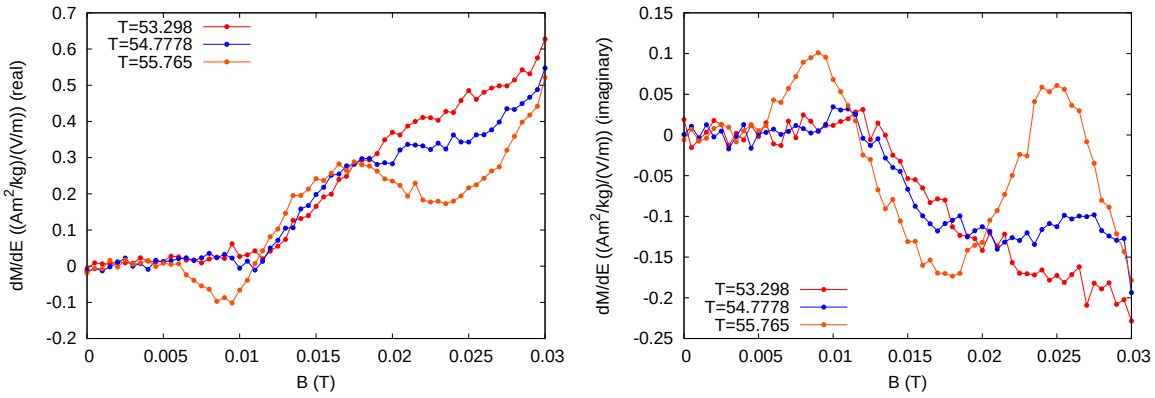

Fig. 3. *dM/dE vs magnetic field at different temperatures for $T < 56\ K$. The first figure shows the variation of the real part of dM/dE while the second figure shows the imaginary part*

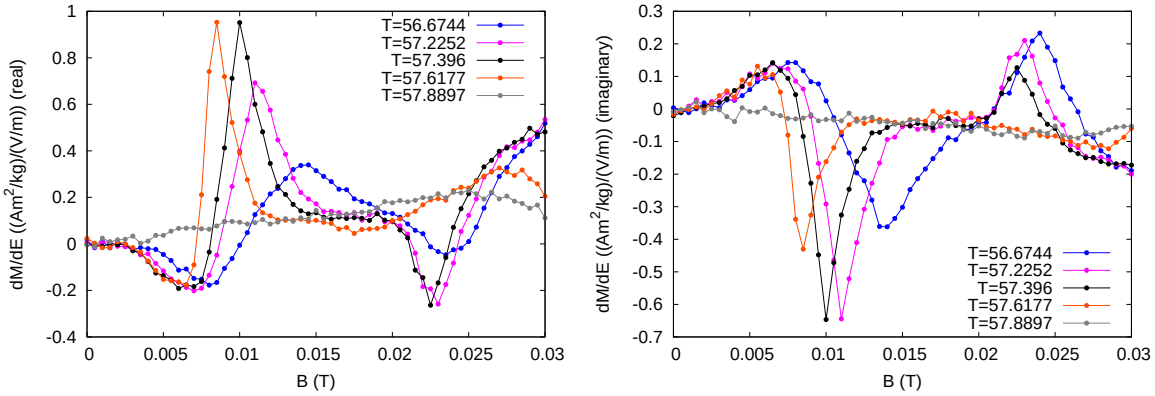

Fig. 4. *dM/dE vs magnetic field at different temperatures for $56\ K < T < 58\ K$. The first figure shows the variation of the real part of dM/dE while the second figure shows the imaginary part*

K and 58 K. This is the temperature range where skyrmion phase exists. The transition from helical (nearly zero dM/dE) to the skyrmion phase is clearly marked by the peak at $B \sim 0.01\ T$, and the transition from the skyrmion to the conical phase is marked by the dip at $B \sim 0.025\ T$. The conical phase can again be identified by increasing dM/dE signal with magnetic field. This is consistent with the observation made in Omrani et al. (2014). The imaginary part of dM/dE also shows similar pattern but with a dip at $B \sim 0.01\ T$ and a peak at $B \sim 0.025\ T$ which is just opposite to the real part's behaviour. Thus the skyrmion phase is seen to appear around 56.5 K and then again disappear around 58 K where there is the transition to the ferrimagnetic phase. To demonstrate this, figure 6 shows the real and the imaginary part of dM/dE together at $T \sim 57\ K$.

As the temperature approaches $\sim 58\ K$ and goes above it, the dM/dE signal becomes very small and almost zero as shown in figure 5. This is because above 58 K, Cu_2OSeO_3 goes into ferrimagnetic phase which doesn't show ME coupling.

Thus the ME susceptibility shows distinct responses in different magnetic phases of Cu_2OSeO_3

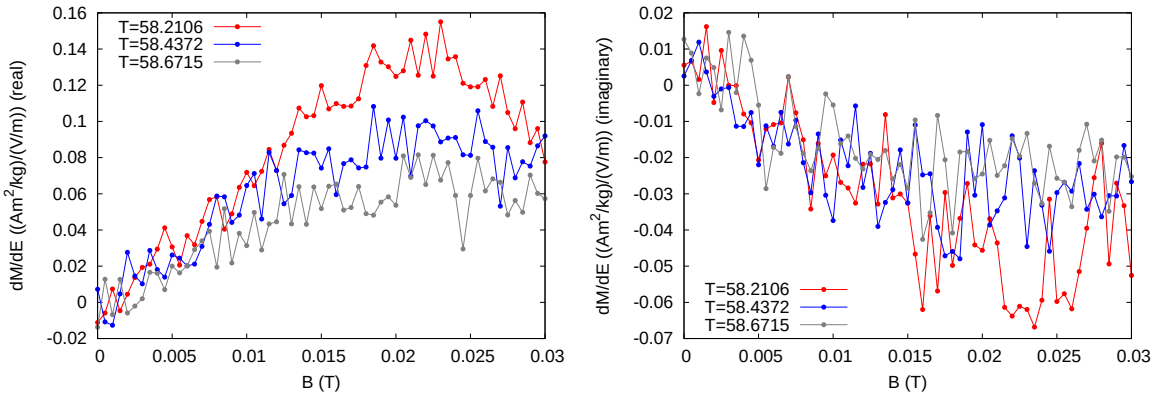

Fig. 5. *dM/dE vs magnetic field at different temperatures for $T > 58\ K$. The first figure shows the variation of the real part of dM/dE while the second figure shows the imaginary part*

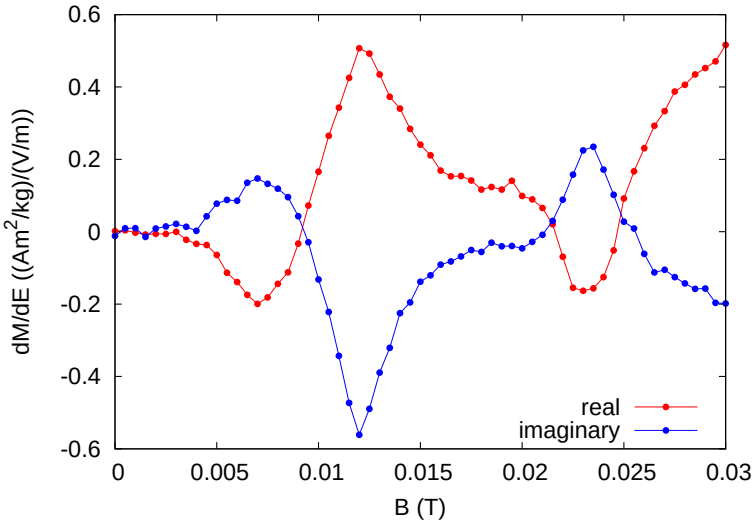

Fig. 6. *dM/dE vs magnetic field at $T = 57\ K$ for both the real and imaginary parts*

and at the phase boundaries as well. Thus it can be used to construct the magnetic phase diagram of Cu_2OSeO_3 by measuring ME susceptibility at different temperatures and magnetic fields. Figure 7 shows the phase diagram constructed using the real as well as the imaginary parts of dM/dE. It can be seen that the helical, conical, ferrimagnetic and skyrmion phases are clearly visible on the phase diagram. The helical and ferrimagnetic phases have very low (nearly zero) value of dM/dE, while the conical phase has some finite value whose real part increases with magnetic field. And the phase boundaries with the skyrmion phase, marked by the peaks and dips in both the real and imaginary dM/dE phase diagram, are also clearly visible in the figures. The phase diagram is similar in the trends to that given by Omrani et al. (2014) although for different directions of B and T i.e similar kind of behaviour of the dM/dE signal at different B and T have been observed here. This include very small signal in the helical and ferrimagnetic phase, increasing trend of dM/dE with B in the conical phase and sharp peaks and dips in the dM/dE at the

boundaries of the skyrmion phase. Figure 8 shows the magnetic phase diagram showing the different phases - helical, conical, skyrmion as given by Omrani et al. (2014).

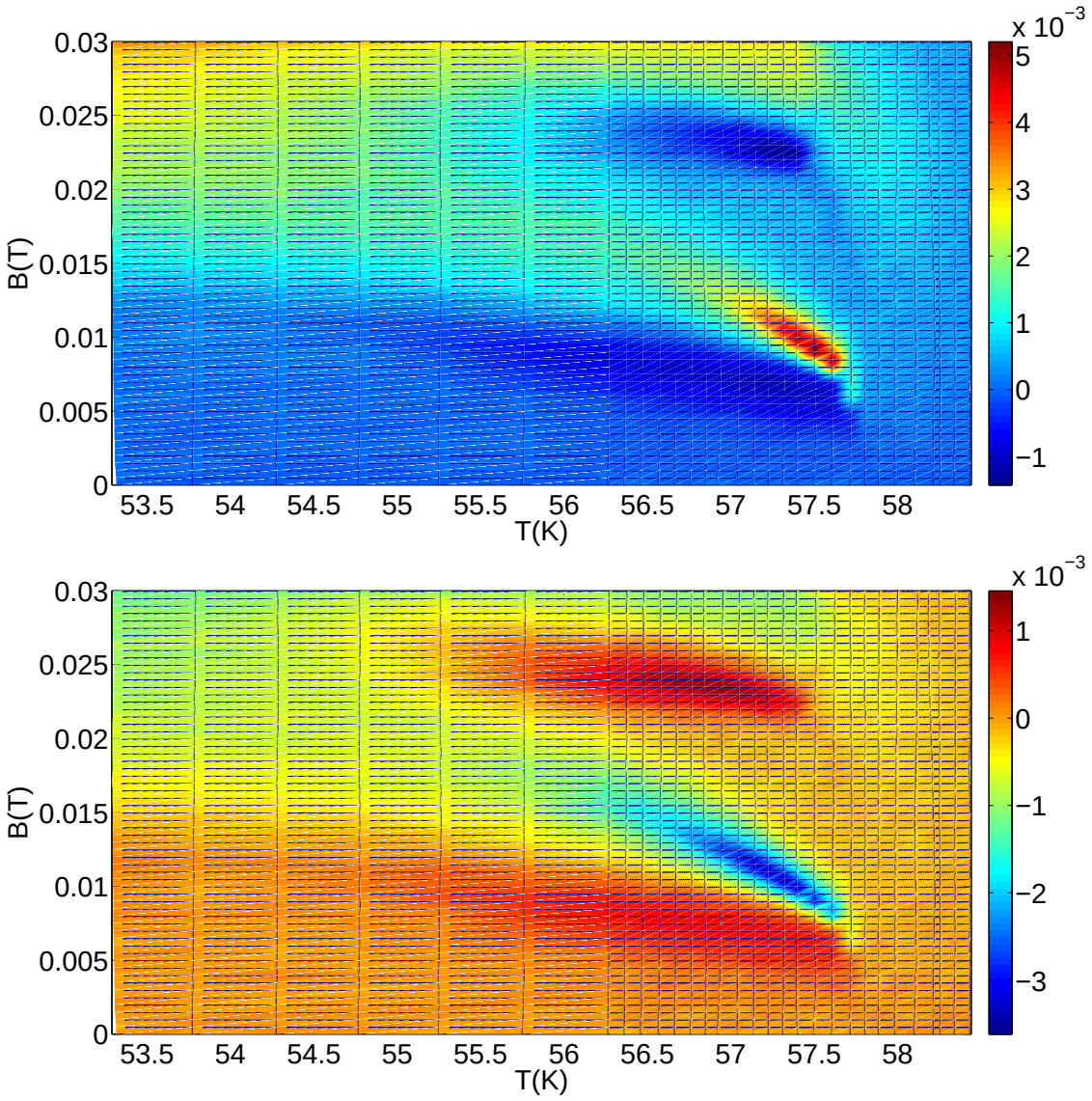

Fig. 7. *Phase Diagram for* Cu_2OSeO_3 *with ME susceptibility (dM/dE). The first figure is for the real part of dM/dE while the second figure is for the imaginary part*

Thus the AC magnetoelectrical susceptibility study for Cu_2OSeO_3 has been successful in obtaining a good phase diagram. Thus attempts can be now made to observe the same AC ME susceptibility signals in rare earth manganites $TbMnO_3$ and $DyMnO_3$. But at first DC magnetization measurements should be performed on them to get an idea of the different transition temperatures in them. These studies are described in detail in the following section.

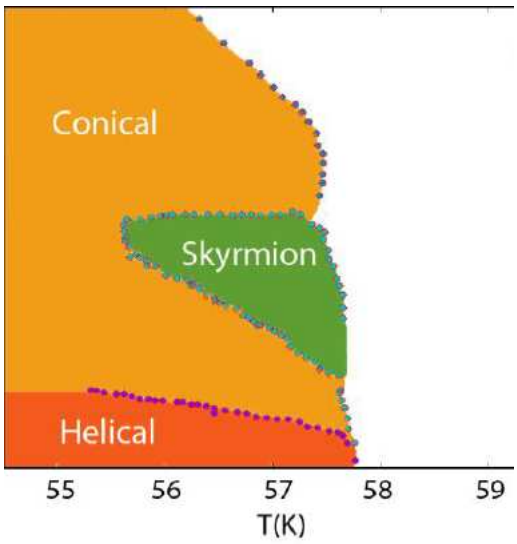

Fig. 8. *Portion of the magnetic phase diagram near the ordering temperature extracted from the real part of the temperature scans signals as given by Omrani et al. (2014)*

3 DC (M-T) and dM/dE measurements for the Rare Earth Manganites

Rare earth manganites like $TbMnO_3$ show strong ME coupling as already discussed in previous sections, exhibiting strong dependence of the the electric polarization on the magnetic field as described in Kimura et al. (2003), Goto et al. (2004) and Kimura et al. (2005). Following success of the dM/dE technique on Cu_2OSeO_3, the same can be attempted on rare earth manganites. The following subsections describe the preparation of the samples followed by DC magnetization measurements and finally attempts to measure the ME susceptibility or dM/dE.

3.1 Sample Characterization

Both $TbMnO_3$ and $DyMnO_3$ have an orthorhombically distorted perovskite crystal structure in the space group of *Pbnm*. The lattice parameters are given in Table 1.

Table 1
Lattice parameters for $TbMnO_3$ *and* $DyMnO_3$

	a (Å)	b (Å)	c (Å)
$TbMnO_3$	5.297	5.831	7.403
$DyMnO_3$	5.275	5.828	7.375

The sample pieces present were of arbitrary shape and thus they needed to be aligned by the X-Ray Laue method to know the three crystal axis directions i.e. [100] i.e. a-axis, [010]

i.e. b-axis and [001] i.e. c-axis, and then cut along those surfaces to get regularly shaped sample pieces.

At first $TbMnO_3$ was aligned using X-Ray Laue and the three above mentioned axis directions were determined. Figure 9 shows the Laue patterns for these three orientations. After obtaining the crystal axis directions, the sample piece was cut along surfaces perpendicular to these directions using a wire-saw. Cutting the sample to make a smaller piece was also required to avoid rotation of the sample inside the sample chamber of the SQUID.

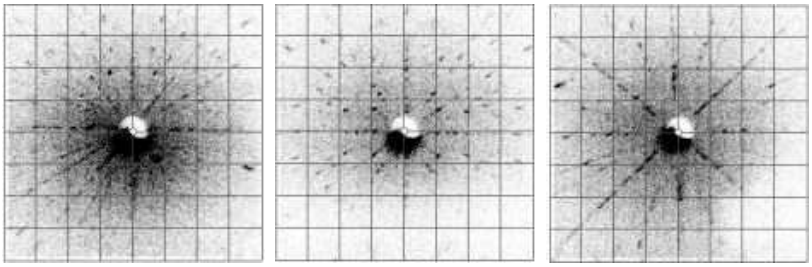

Fig. 9. *Laue patterns for* $TbMnO_3$. *The first figure is for* [100] *i.e. a-axis direction, the second figure is for* [010] *i.e. b-axis directions and the third figure is for* [001] *i.e. c-axis direction. The X-Rays were produced using V=20 kV and I=50 mA in the power supply*

Finally after the cutting, the sample piece has the rectangular shape as shown in figure 10. The dimensions of the piece are also shown in the figure. The mass of this sample was measured to be 11.6 mg.

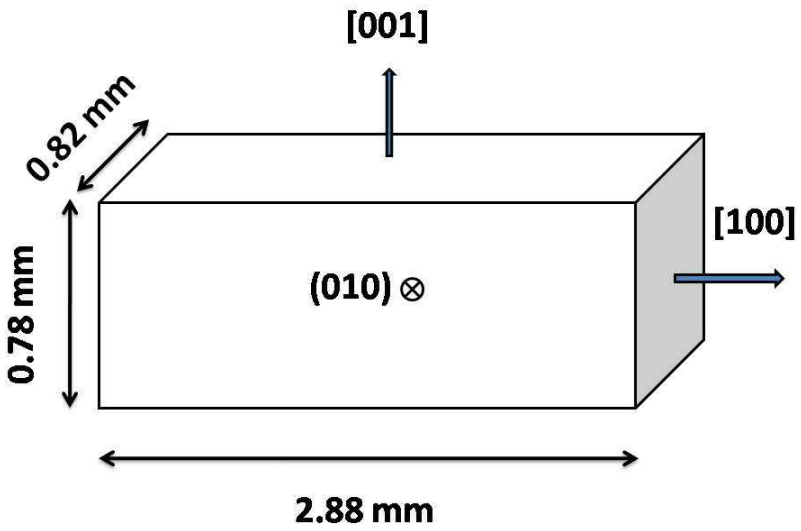

Fig. 10. *Shape of the* $TbMnO_3$ *sample piece with the axis directions.* [100] *corresponds to a-axis,* [010] *corresponds to b-axis and* [001] *corresponds to the c-axis*

The same procedure was repeated for the $DyMnO_3$ sample piece. Figure 11 shows the Laue patterns for $DyMnO_3$. After orienting it was also cut along the surfaces normal to these directions to obtain a rectangular piece as shown in Figure 12. The mass of this sample was measured to be 17.8 mg.

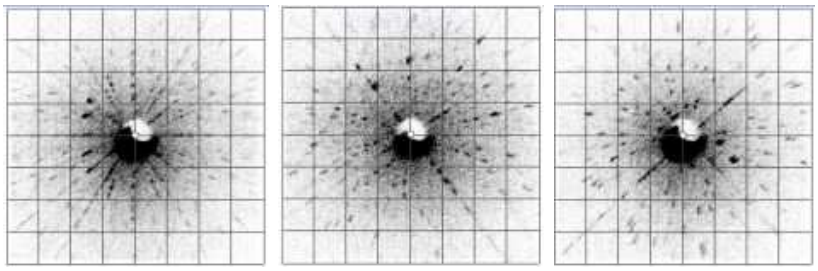

Fig. 11. *Laue patterns for* $DyMnO_3$. *The first figure is for* [100] *i.e. a-axis direction, the second figure is for* [010] *i.e. b-axis directions and the third figure is for* [001] *i.e. c-axis direction. The X-Rays were produced using V=20 kV and I=50 mA in the power supply*

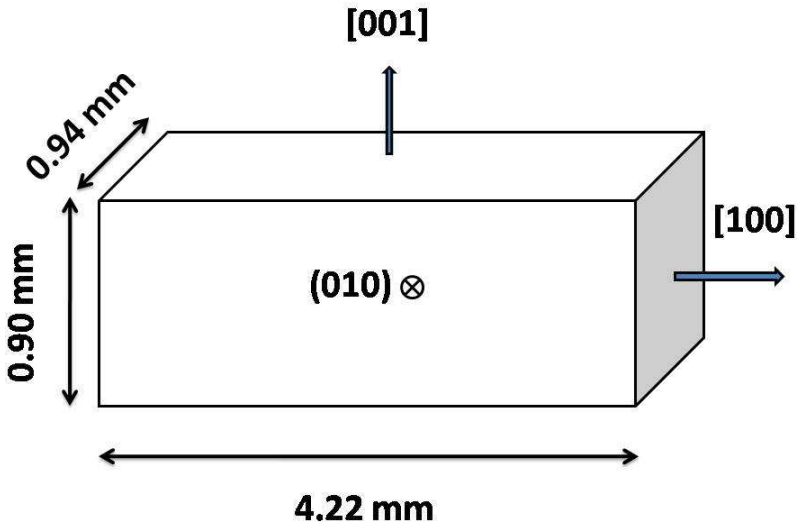

Fig. 12. *Shape of the* $DyMnO_3$ *sample piece with the axis directions.* [100] *corresponds to a-axis,* [010] *corresponds to b-axis and* [001] *corresponds to the c-axis*

Thus now both $TbMnO_3$ and $DyMnO_3$ samples have been oriented and cut for the DC magnetization (M-T) and ME susceptibility measurements. Therefore, electric and magnetic field can now be applied along known crystal axes to carry out the measurements.

DC magnetization measurements were carried out for both $TbMnO_3$ and $DyMnO_3$ to observe the temperature variation of magnetization. Since the crystal axes directions are now known, M-T measurements along all the three axes i.e. [100], [010] and [001] were performed. Since both the samples are paramagnetic above $\sim 41 - 42\ K$, a degaussing process at 70 K was performed to remove any remnant magnetization. The sample was then first cooled to 5 K at zero field (ZFC) and then a temperature scan performed by applying a DC magnetic field of H=5000 Oe (=0.5 T) till 70 K with greater number of observations near the known transition temperatures (given in Section 1.2). The degaussing process was repeated and the sample was then cooled to 5 K in presence of the magnetic field (FC). The same temperature scan was then performed till 70 K.

Figures 13 and 14 show the M-T measurements for all the three axes (ZFC and FC) for $TbMnO_3$ and $DyMnO_3$ respectively.

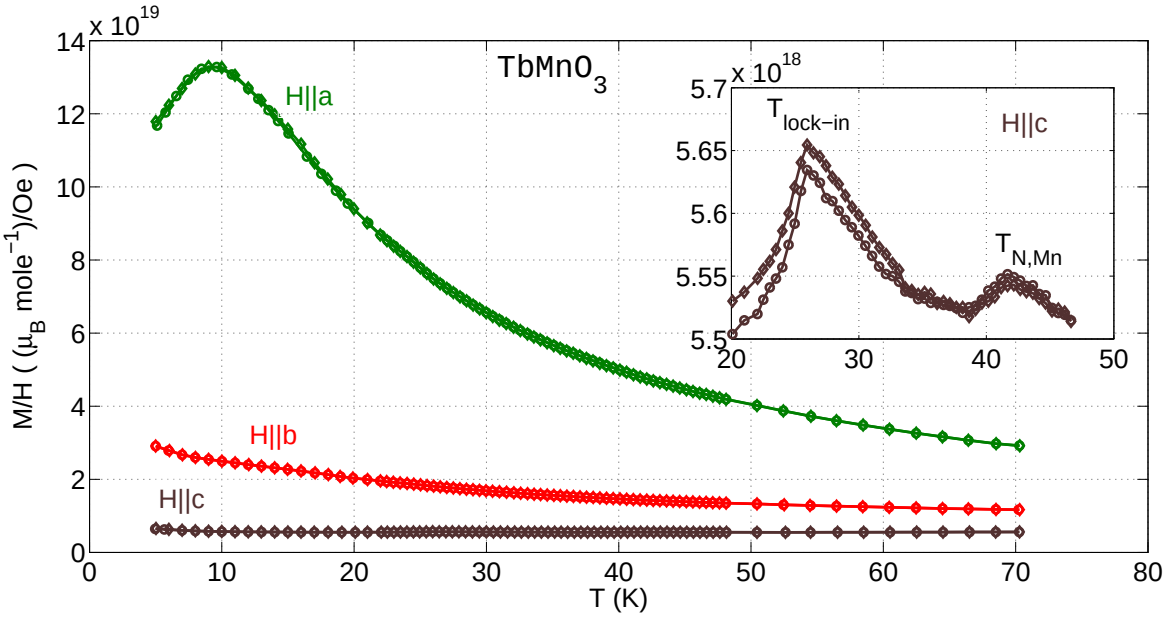

Fig. 13. *Magnetization vs Temperature curve for* $TbMnO_3$. *Magnetization measurements along different crystal axes are marked by different colours. All measurements were performed at* $H = 5000$ *Oe. Circles are used to mark Zero Field Cooled (ZFC) measurements and diamonds are used to mark Field Cooled (FC) measurements.*

The observations for $TbMnO_3$ match quite well with the data given by Flynn et al. (2014) for DC M-T measurements along all three axes. For $TbMnO_3$ it can be seen that along the a-axis, only the ordering of the Tb^{3+} ions is visible which shows antiferromagnetic behaviour below the transition temperature for Tb^{3+} at 8 K and paramagnetic behaviour above it. Also the magnetic moment is largest along this direction thus showing that the

Tb^{3+} ions lie preferentially along this axis at low temperatures. Along the b-axis, only the paramagnetic behaviour is observed.

C-axis is the only axis along which signatures in susceptibility ($\chi = M/H$) were obtained for the transitions due to ordering of Mn moments. The susceptibility shows a general paramagnetic behaviour but with peaks at 26 K and 42 K. The paramagnetic behaviour is due to the large magnetic moment of the Tb^{3+} moments while the peaks are obtained due to the Mn moments. The peak at 42 K corresponds to the Neel temperature for Mn ($T_{N,Mn}$) while the peak at 26 K marks the lock-in temperature ($T_{lock-in}$) at which spontaneous electric polarization appears in $TbMnO_3$. This also matches with the observation given by Kimura (2007). Also along the a and b-axis the susceptibility is identical for ZFC and FC while for the c-axis there is some amount of hysteresis between ZFC and FC.

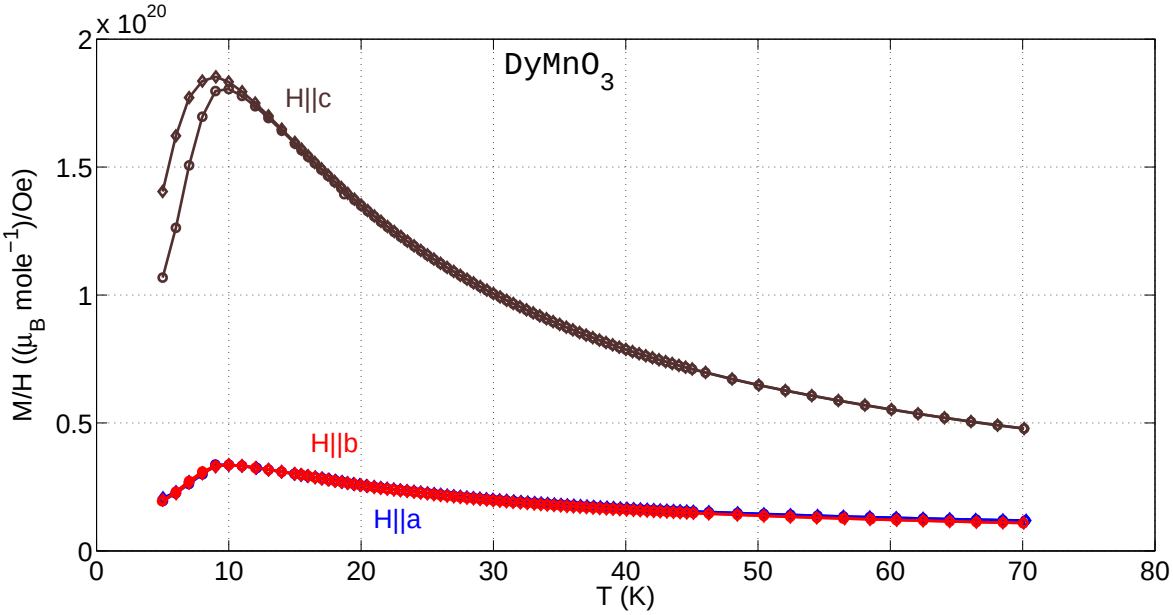

Fig. 14. *Magnetization vs Temperature curve for* $DyMnO_3$. *Magnetization measurements along different crystal axes are marked by different colours. All measurements were performed at H = 5000 Oe. Circles are used to mark Zero Field Cooled (ZFC) measurements and diamonds are used to mark Field Cooled (FC) measurements.*

In $DyMnO_3$, observations along all three axes show the transition from paramagnetic to antiferromagnetic state at 9 K which is due to the ordering of the Dy^{3+} moments. The magnetic moment along the c-axis is much larger than along a and b-axis which may be due to the preferential orientation orientation of the Dy^{3+} moments along the c-axis. In this case, no clear signature in the susceptibility (to indicate the ordering of the Mn moments) was obtained along any of the three axes. Also the susceptibility along c-axis showed a clear hysteresis between ZFC and FC measurements while it was identical for ZFC and FC measurements along both a and b-axis.

Thus clear signatures indicating ordering of Mn moments were observed in $TbMnO_3$, and it is the ordering of the Mn moments with which the magnetoelectric effects in $TbMnO_3$ are associated. Thus dM/dE measurements were first attempted on this $TbMnO_3$ sample which is described in the following section.

3.3 dM/dE measurements for $TbMnO_3$

After the DC magnetization measurements on $TbMnO_3$ and $DyMnO_3$, dM/dE measurements were now attempted on $TbMnO_3$. The experimental setup used has been described briefly in Section 1.5.2. The AC magnetoelectric susceptibility dM/dE is measured by applying an AC electric field using a lock-in amplifier in the same way as measured for Cu_2OSeO_3. In Section 1.4 it has been shown how the output signal from the lock-in amplifier directly gives the linear magnetoelectric susceptibility.

Now for $TbMnO_3$ the sample piece is large enough to have a very high magnetic moment at high magnetic fields (above 3 T) and thus tends to rotate inside the sample tube during the measurements. This hampers the measurements which require the electric and magnetic fields to be applied along specific crystal axis directions. In order to ensure that the sample remains fixed inside the sample tube, cotton and parts of plastic capsule and tubes were used to fix the sample after the soldering the wires to the copper electrodes on the sample. Figure 15 shows how the sample was fixed inside the sample tube.

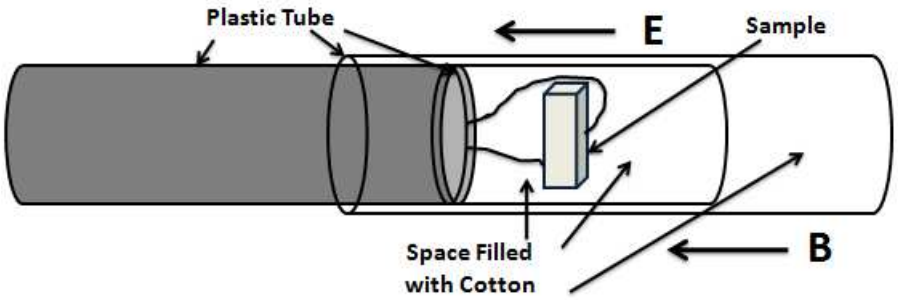

Fig. 15. *Design of the Sample Holder to fix the sample during measurements. The direction of magnetic field is as shown along the sample tube. The electric field can be applied both in the direction shown or perpendicular to it using the wires shown. The empty spaces inside the plastic tubes are filled with cotton to tightly fix the sample.*

This arrangement prevented the sample from rotating at high magnetic fields and thus allowing measurements at these magnetic fields.

3.3.1 Measurements for different orientations and (B,T) combinations

Now attempts were made to observe the dM/dE signal for different orientations of electric and magnetic fields and also at various regions of the phase diagram i.e. at various combinations of magnetic field (B) and temperature (T). This included orientations where electric field (E) and magnetic field (B) were both parallel and perpendicular. The combinations of B and T included regions in the all the different phases in the phase diagram i.e. the incommensurate antiferromagnetic phase ($27 < T < 41$ K), the commensurate anitferromagnetic phase ($T < 27\ K$) and also the paramagnetic phase ($T > 41\ K$). Figure 16 shows the magnetic phase diagram for $TbMnO_3$ (Kimura et al. , 2005) with the regions indicated where the measurements were attempted.

All the dM/dE measurements were done by applying the AC electric field along the c-axis of the crystal. Since $TbMnO_3$ exhibits magnetically induced spontaneous polarization only along the c-axis below its T_{lock_in}, therefore there is maximum chance of the coupling of electric and magnetic properties along this direction. Along b-axis there is no spontaneous polarization for any combination of B and T. Along the a-axis, there is only one configuration which allows spontaneous polarization, but it only occurs for $B > 7\ T$ which is the maximum magnetic field that can be applied using our instrument. Therefore, applying electric field along a or b-axis won't result in any coupling with the magnetic properties in our regime of magnetic field. Apart from that the thickness of the sample along the a-axis is too large and thus will result in very low electric field for a given voltage applied. So, the electric field has been always applied along the c-axis. An AC voltage with a maximum RMS value of 100 V has been applied. The frequency mainly used is 10 Hz, although both higher and lower frequencies have been tested to search for a signal. Almost all the following observations have been done with 100 V AC voltage.

Now for the direction of the magnetic field, at first magnetic field was applied parallel to the b-axis. This was because features in the dM/dE signals are expected near the phase boundaries as seen from the study of Cu_2OSeO_3, and the phase boundary (where the spontaneous polarization flops from c to a-axis)is near 5 T or less at low temperatures which is accessible using our instrument.

So at first, AC electric field parallel to c-axis, and DC magnetic field parallel to b-axis were applied at T=10 K and B=5 T. This is very near to the phase boundary mentioned above and is marked by the red cross in Figure 16. The RMS value of the electric field was increased from 5 V to 100 V during the measurement, but no dM/dE response was observed. An expected signal is a sinusoidal variation in the SQUID signal varying in magnitude with the magnitude of the electric field and a signal from the lock-in amplifier for which the θ varies within ± 2 degrees. No such signal was observed for these orientations and under these conditions. So the next two measurements were attempted at 30 K and 45 K -one in the paraelectric incommensurate antiferromagnetic (AF) phase and the other in the paramagnetic (PM) phase, both for B=5 T . No dM/dE response was observed

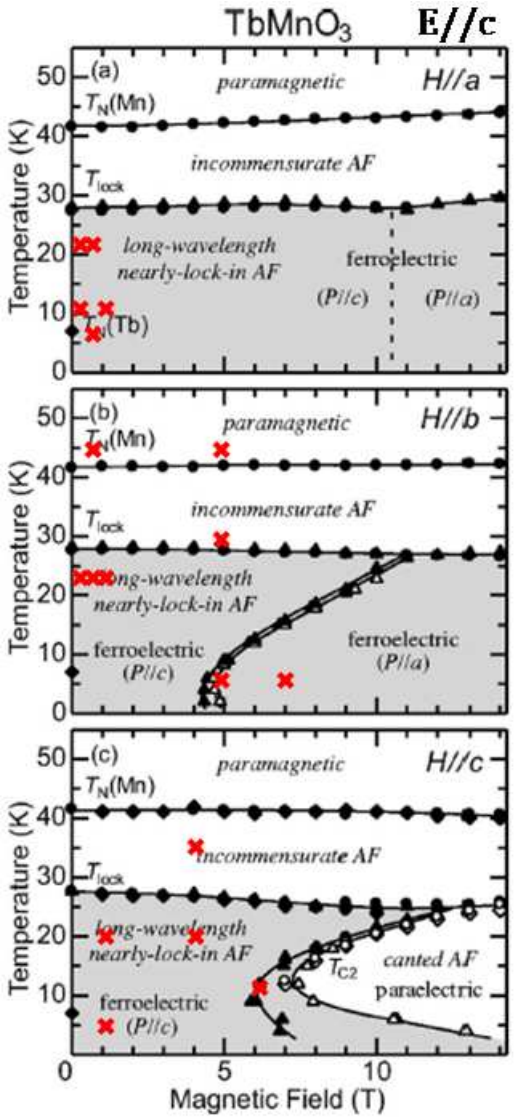

Fig. 16. *Phase Diagram for* $TbMnO_3$ *for magnetic field along all three axes and electric field along the c-axis. The red crosses on each phase diagram marks the magnetic field and temperature where dM/dE measurements were attempted. The phase diagram has been taken from Kimura et al. (2005)*

in these cases either. One reason could be that since at this field a large spontaneous polarization already exists along the c-axis, a small change due to the AC E-field might not be sufficient to cause a change in the spin ordering so as to have an effect on the magnetization. Therefore, the next measurement was attempted at T=10 K and B=7 T, such that $TbMnO_3$ is now in the phase where the polarization (P) has flopped (Kimura , 2007) to the a-axis. But still there was no response.

A possible reason for this might be that at the high magnetic fields applied, the spins may be frozen and thus the little change in polarization is not sufficient to affect the ordering

of the spins. Therefore, measurements were then tried at low B values - T=25 K & B=0 T, T=25 K & B=0.1 T and T=25 K & B=1 T which is in the ferroelectric phase with $P \| c$ and T=45 K & B=1 T which is in the PM phase. There was no dM/dE response observed in this case as well.

Now in $TbMnO_3$, as given by Kimura (2007) the Mn moments are arranged in a non-collinear spin structure namely cycloidal structure. Here the spins rotate in the b-c plane such that the rotation axis is along the a-axis and the propagation vector of the spiral is along the b-axis. And therefore, the spontaneous polarization induced magnetically is along the c-axis. Also in this phase i.e. $T < 27\ K$, the magnetoelectric coupling is due to the Mn moments, the Tb^{3+} ions play no role. This phase is antiferromagnetic for Mn and thus there is no net magnetization (M) in the cycloidal phase. But if a magnetic field is applied along the c-axis, then the spin structure becomes conical (Kimura , 2007), and there is now a non-zero component of M along the c-axis. Now since P can only interact with the Mn ions, and as it was the conical phase which had previously given promoinent dM/dE response in $TbMnO_3$, therefore, the new orientation tried was - $E \| c$ and $H \| c$.

The measurement in this orientation was at T=5 K and B=1 T. The temperature is below the Tb ordering temperature ($\sim$7K) but is in the ferroelectric phase with $P \| c$, but still there was no dM/dE response observed neither in the lock-in nor in the SQUID output. Next, measurements at T=20 K & B=1 T and T=20 K & B=4 T were also attempted but yielded no results. These two were in the same phase as the previous one. Next, one measurement was done in the paraelectric incommensurate AF phase i.e. T=35 K & B=4 T, but still no response was observed. Finally for this orientation, measurement was done at T10 K & B=6 T which is exactly near the phase boundary as shown in Figure 16, and the transition is into a phase where $P \| c$ is suppressed, thus allowing the little change in polarization to become significant. This measurement also did not show any positive response from the sample.

Since this orientation also did not result in any dM/dE response, the final orientation - $E \| c$ and $H \| a$ was prepared for the next measurement. All the measurements for this orientation have been done for the same phase of $TbMnO_3$ as shown in the figure - T=10 K & B=1 T, T=10 K & B=0.01 T, T=20 K & B=0.01 T, T=20 K & B=0.5 T and T=5 K & B=0.5 T. The last measurement was below the Tb transition temperature. In all these cases, as before no dM/dE response was observed neither from the SQUID output, nor the lock-in amplifier.

Therefore, several measurements in search for the dM/dE signal have been performed in different regions of the phase diagram and for E along the c-axis, but no dM/dE response has been detected. As already discussed above, applying E along a or b-axis should also not give any dM/dE signal. Further discussions on this absence of dM/dE signal in $TbMnO_3$ is given in the following subsection.

3.3.2 Absence of dM/dE response and Discussions

According to the experiments performed here, $TbMnO_3$ was not found to show any dM/dE response in any of its phases. There may be different reasons possible for this absence of dM/dE response. One such reason can be described as follows. In Cu_2OSeO_3, there is a known relation between P and B (Seki et al. , 2012). Therefore P varies with B and the vice cersa should also be true, i.e. magnetization M should also change with E. As a result, dM/dE signal has been observed in Cu_2OSeO_3. On the other hand in $TbMnO_3$ there is no such known relation between P and B. The only effect that magnetic field has on polarization is the flopping of the polarization from one axis to the other and also the suppression of polarization. The spontaneous polarization P_c is saturated along the c-axis from 0 magnetic field (for $T < T_{lock-in}$) and suddenly flops to the a-axis at certain value of magnetic field or gets suppressed depending on the direction of the applied magnetic field. There is no continuous variation of P with B. So it is possible that there is no continuous variation of M with E either. And since the experimental technique here measures the change in M with E, this may be the reason for absence of dM/dE response.

Also in the small region during the flopping, where there might be some variation in P with B, the thermal fluctuation energy is seen to be higher than the interaction energy of P with E. So this doesn't allow for the change in polarization due to the AC electric field to result in a change in the magnetization. Therefore, the combined effect of these factors might be the reason that dM/dE measurements were not observed in $TbMnO_3$.

Since $DyMnO_3$ has similar magnetic magnetic structure as well similar magnetoelectric coupling and phase diagram, therefore dM/dE measurements were not attempted on $DyMnO_3$. This technique of AC magnetoelectric susceptibility can be instead applied on materials which have some known variation of polarization with magnetic field. Examples of such materials are Cr_2O_3 and R_2CuO_4 (R=Gd, Sm, Nd and La). In all these materials, P is 0 and not saturated at $B = 0$, and also shows some continuous variation (linear or non-linear) with B. These features were absent in $TbMnO_3$. Thus these materials suggested above may be used to carry out further AC magnetoelectric susceptibility measurements.

4 Summary

During this short-term summer project, the AC Magnetoelectrical Susceptibility measurement technique has been investigated for Cu_2OSeO_3 as well as a rare earth manganite - $TbMnO_3$. The method has been quite successful in Cu_2OSeO_3 where clear dM/dE response has been observed in different magnetic phases and also there were sharp features at the phase boundaries. Thus it was possible to carry out a sensitive probe of the magnetic phase diagram using this technique. On the other hand for $TbMnO_3$, this technique was not successful as no dM/dE response was observed for different orientations and several

conditions of magnetic field and temperature. $TbMnO_3$ along with another rare earth manganite $DyMnO_3$ samples were prepared by first orienting using the X-Ray Laue method and then by cutting the crystal along the determined crystal axis directions. DC magnetization measurements were also performed on both of them to study the variation of magnetization with temperature. The results for $TbMnO_3$ were compared with previously known results and they showed reasonable match. Several regions of the magnetic phase diagram of $TbMnO_3$ were then probed by applying an AC magnetic field in search of the dM/dE response but it could not observed. As a continuation of this work, this technique can be tried on $DyMnO_3$ once as well. Other areas of the phase diagram for $TbMnO_3$ can also be probed. Also the crystal axis directions and DC magnetization measurements for $DyMnO_3$ may once be repeated to confirm with some known results. Apart from that other materials like Cr_2O_3 and R_2CuO_4 as mentioned above can also be taken to study this technique.

5 Acknowledgment

I would like to thank my project supervisor Prof. Henrik Ronnow for providing me this opportunity to work on an experimental project on a very interesting topic in condensed matter physics - magnetoelectric susceptibility studies of multiferroics and for his help, suggestions and guidance during my project work. I would also like to thank Mingee and Ping for their immense help and guidance throughout the duration of the project and explaining to me different aspects of the subject, which helped me in gaining a much better understanding of my work. I would also like to thank Claudia and Julian for their help and guidance during my work and for the understanding of different experimental techniques. I would like to thank again all the group members of LQM for helping me gain deep insights into this field and making my experience in experimental physics at LQM so rich and valuable for my future. I would also like to express my gratitude to Ecole Polytechnique Federale de Lausanne (EPFL) for providing me this opportunity to work in this prestigious institute and for this wonderful exposure to research in condensed matter physics.

References

T.Kimura Annu. Rev. Mater. Res. 2007. 37:387413

W. Eerenstein, N. D. Mathur, J. F. Scott, Nature, Vol 442—17 August 2006 doi:10.1038/nature05023

S. Seki, S. Ishiwata and Y. Tokura, Physical Review B 86, 060403(R) (2012)

T.Kimura, T.Goto, H. Shintani, K.Ishizaka, T.Arima and Y.Tokura, Nature. Vol 426, 6 November 2003

T. Goto, T. Kimura, G. Lawes, A. P. Ramirez, and Y. Tokura, Physical Review Letters, Vol 92. Number 25, 2004

T.Kimura, G.Lawes, T.Goto, Y.Tokura and A.P.Ramirez, PHYSICAL REVIEW B 71, 224425 (2005)

A.A.Omrani, J.S.White, K.Pra, I. ivkovi, H. Berger, A. Magrez, Ye-Hua Liu, J. H. Han, H. M. Rnnow, Phys. Rev. B 89, 064406 (2014)

Dzyaloshinskii I. 1958. J. Phys.Chem. Solids 4:24155

Moriya T. 1960. Phys. Rev. 120:9198

D O'Flynn, M R Lees and G Balakrishnan 2014. J. Phys.: Condens. Matter 26 (2014) 256002 (6pp)

M. Kenzelmann, A. B. Harris, S. Jonas, C. Broholm, J. Schefer, S. B. Kim, C. L. Zhang, S.W. Cheong, O. P. Vajk, and J. W. Lynn, PRL 95, 087206 (2005)

6 Appendix

6.1 Sample alignment using Laue

The alignment of the samples are done using the X-Ray Laue method in order to determine the orientation of the crystals. The diffracted beams from the cruystal form arrays of spots, which lie on curves on the film. Now since the Bragg angle is fixed for every set of planes in the crystal, each set of planes diffracts the particular wavelength from the white radiation that satisfies the Bragg law for the values of d (inter-planar distance) and q (wave-number $|q| = \frac{2\pi}{\lambda}$) involved. Each curve therefore corresponds to a different wavelength. There are two practical variants of the Laue method, the back-reflection and the transmission Laue method. Here the back-reflection Laue method has been used. In the back-reflection method, the film is placed between the x-ray source and the crystal. The beams which are diffracted in a backward direction are recorded and the diffraction spots generally lie on

an hyperbola on the film.

X-Ray Laue method was used to determine the orientation of the Cu_2OSeO_3 crystal as well as of the rare earth manganites - $TbMnO_3$ and $DyMnO_3$. The sample can be moved vertically, horizontally, slanted up and down, rotated in the horizontal as well the vertical plane in order to orient it. The horizontal and vertical movement is used to control the postion of the sample such that the X-ray falls on it. In the Laue image, slanting up, down and rotation in the horizontal plane corresponds to translation of the pattern of spots obtained. Rotation of the sample in the vertical plane perpendicular to the incident X-ray corresponds to rotation of the pattern in the Laue image. The samples were therefore aligned using these controls in order to obtain the correct Laue pattern for the different crystal axis. The patterns were matched with Java Laue to determine the correct pattern for each orientation. The Laue patterns obtained for the different orientations of these crystals are shown in the above sections.

After the alignment of the crystal it sometimes needs to be cut along these directions to obtain a regular shape of the sample. This was required for the $TbMnO_3$ and $DyMnO_3$ crystals in this case. After alignment the sample is then fixed to a goniometer using wax and then aligned once again at the same position with the X-Ray. This is required to be able to cut the crystal along the desired surface.

6.2 Sample Cutting

The sample after being aligned using the X-Ray Laue method and attached to the goniometer, requires to be cut along the desired surface. The cutting in this case was done using a Wire Saw. The goniometer is attached to the instrument and the wire of the wire saw is placed on top of the sample. In this arrangement, the wire is exactly parallel to the surface desired to be cut. Drops of SiC powder mixed with oil is put on the wire and the sample. Silicon carbide is an excellent abrasive and it is required for the wire to cut through the sample. The wire then moves to and fro and presses down on the sample continuously thus cutting it over a period of time. Without any kind of external vibration or disturbance this method produces very smooth surfaces of the crystal.